JOURNAL OF APPLIED PHYSICS **105**, 014911 (2009)

A mixed finite element/boundary element approach to simulate complex guided elastic wave periodic transducers

S. Ballandras,[1,a)] R. Lardat,[2] M. Wilm,[3] Th. Pastureaud,[2] A. Reinhardt,[4] N. Champavert,[1] W. Steichen,[5] W. Daniau,[1] V. Laude,[1] R. Armati,[1] and G. Martin[1]
[1]*FEMTO-ST, UFC-ENSMM-UTBM, UMR CNRS 6174, F-25044 Besançon Cedex, France*
[2]*THALES Underwater Systems, 525 Route des Dolines, F-06903 Sophia Antipolis Cedex, France*
[3]*IMASONIC SAS, ZA Rue des Savourots, 70190 Voray sur l'Ognon, France*
[4]*CEA-LETI, 17 Avenue des Martyrs, 38054 Grenoble Cedex 9, France*
[5]*THALES Safare, 525 Route des Dolines, F-06903 Sophia Antipolis Cedex, France*

(Received 28 April 2008; accepted 4 October 2008; published online 13 January 2009)

The development of new surface acoustic wave devices exhibiting complicated electrode patterns or layered excitation transducers has been favored by an intense innovative activity in this area. For instance, devices exhibiting interdigital transducers covered by piezoelectric or dielectric layers have been fabricated and tested, but the design of such structures requires simulation tools capable to accurately take into account the actual shape of the wave guide elements. A modeling approach able to address complicated surface acoustic wave periodic structures (defined in the saggital plane) exhibiting any geometry then has been developed and implemented. It is based on the combination of a finite element analysis and a boundary element method. A first validation of the computation is reported by comparison with standard surface wave devices. Surface transverse wave resonators covered by amorphous silica have been built and consequently used for theory/experiment assessment. Also the case of recessed electrodes has been considered. The proposed model offers large opportunities for modeling any two-dimensional periodic elastic wave guide. © *2009 American Institute of Physics*. [DOI: 10.1063/1.3021307]

I. INTRODUCTION

The simulation of periodic interdigital transducers (IDTs) devoted to surface acoustic wave (SAW) applications has received a very high interest for more than ten years. From the very pioneer works by Engan[1] to the advanced modeling tools by Ventura *et al.*,[2] strong efforts have been developed to improve the understanding of the excitation and guiding wave phenomena in SAW devices, thus favoring the arising of a SAW device industry providing high quality filters, resonators, and sensors used worldwide. Along the corresponding years of scientific and technical developments, one has to acknowledge the contributions by Blötekjaer *et al.*,[3] introducing for the first time the notion of strip admittance, later generalized by Zhang *et al.*[4] as the harmonic admittance, and then the first combinations of finite element analyses (FEA) together with boundary integral methods (BIMs) achieved by Baghaï-Wadji and co-workers[5,6] allowing to take into account the actual shape of electrodes used to excite and detect the surface waves. Many research groups have followed and improved these first attempts, yielding for instance the generalization of periodic Green's-function notions by Plessky and Thorvaldsson[7] and then providing an intensive analysis of all kinds of waves that can be excited and guided by surfaces loaded with any kind of electrodes (Endoh *et al.*,[8] Koskela *et al.*,[9] and Biryukov and Weinhardt[10]). This so-called FEA-BIM approach has also been extended to elastic waves excited on stratified media.[11] As mentioned previously, these very accurate models have been widely and intensively used to compute SAW excitation and propagation parameters,[12] efficiently used in COM or mixed matrix procedures devoted to SAW filter design.

However, the use of advanced transducer structures has revealed many advantages for more robust devices exhibiting optimized properties (for instance, IDTs protected by an insulating layer,[13] IDTs combining grooves and strips,[14] or temperature and leakage compensation on lithium tantalate cuts using an appropriate silica layer[15]). Most of the above-mentioned simulation tools are implemented assuming a single electrode (or maximum of three electrodes[16]) per period deposited on flat surfaces with vacuum as the adjacent medium. This assumption considerably simplifies the model (the electrode is assumed perfectly flat electrically) but is not suited to simulate devices based on more complicated electrode arrangements including dielectric or piezoelectric layers deposited on the electrode array.

Some works have been already developed to enhance the kinds of problem addressed by such models, for instance, based on finite difference and normal mode approaches.[17] In the present work, we propose a general and polyvalent method to simulate any kind of SAW transducer provided its geometry can be defined in the saggital plane. The present paper describes an approach mixing FEA techniques and a boundary element method (BEM) to simulate any periodic two-dimensional (2D) elastic wave guide. The basic idea consists in meshing the nonhomogeneous part of the transducer (typically the domain close to the electrodes) and a very small part of the substrate and the top adjacent medium when required (typically much less than one wavelength). Periodic boundary conditions are considered at the edges of

---

[a)] Electronic mail: sylvain.ballandras@femto-st.fr.

© 2009 American Institute of Physics

the meshed period and a radiation condition then is applied at the meshed boundaries normal to the axis along which lies the periodicity. The corresponding formulation relies on boundary elements built using Green's functions of the substrate and of the adjacent medium. These two domains can be composed of a single material or layered structures (including viscous fluids and metals[18]) assuming flat boundaries.

This FEA-BEM approach is well suited to address different kinds of problems which are generally reduced to ideal cases, thus generating discrepancies between the model and the actual devices. The proposed model provides, for instance, a comprehensive representation of the contribution of the adjacent medium to the static capacitance of standard SAW devices; it is also capable to take into account mass loading and guiding effects due to the deposition of dielectric films above the IDTs or to simulate the elastic contribution of the electrodes in the case of interface waves.[19]

In this section, theoretical developments are detailed together with numerical implementation considerations. Convergence tests have been performed to define the optimal conditions of the computation in terms of accuracy and computation duration. Validation tests then are reported, performed for standard SAW devices on quartz (true SAW and transverse SAW) and lithium tantalate [leaky or pseudo-SAW (PSAW)]. The validation procedure consists in the comparison of numerical results provided by the proposed approach with those delivered by the approach of Ventura *et al.*[2] More complicated structures then are considered to illustrate the capabilities of our model and compared to experiments to validate the efficiency of the proposed approach. A Love wave device consisting of a surface transverse wave (STW) device covered with an amorphous silica layer has been fabricated and its electrical response is compared to the harmonic admittance, demonstrating the capability of the model to accurately predict the resonance frequencies of the experimental device. Finally, the case of recessed electrodes for STW has been addressed, and the predicted band gap amplitude is compared to experimental values,[20] providing again a supplementary validation of the proposed approach. Extensions of the model to more comprehensive analyses finally are discussed as a conclusion of the present paper.

II. FUNDAMENTALS

Figure 1 shows a general scheme of the considered periodic device geometry. Propagation is assumed taking place along x_1. The wave guide is assumed inhomogeneous at the excitation surface (along x_1 and x_2) and the problem independent of x_3. As shown in this figure, the meshed region can be composed of various materials with arbitrary shapes assuming they can be well represented using an elastic-displacement-based FEA formulation. Material losses can also be considered by assuming complex elastic, piezoelectric, and dielectric coefficients.

The basic equations governing periodic FEA computations are now briefly recalled. We consider the case of infinite periodic structures driven by a harmonic electric excitation[4,11,13] yielding the following form of the potential ϕ applied to the electrode:

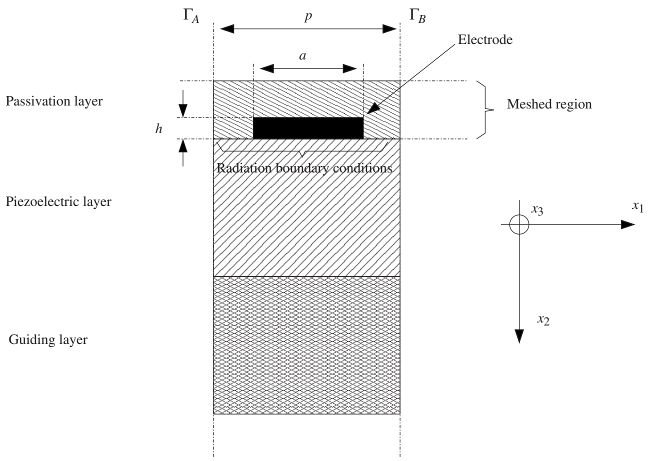

FIG. 1. Typical geometry of elastic wave guides considered in the proposed work.

$$\phi_n = \phi_0 e^{-j2\pi\gamma n}. \tag{1}$$

This signifies that the nth active electrode is excited by a potential of magnitude ϕ_0 modulated by a phase proportional to its distance from the zeroth (reference) electrode. The excitation parameter γ denotes the way the structure is excited. For instance, an integer value of γ corresponds to a synchronous excitation whereas $\gamma=1/2$ holds for an alternate $+V/-V$ excitation of the array. We then only consider the zeroth electrode for the analysis of the grating spectral properties.

As already reported in many references (see, for instance, Refs. 21 and 22), FEA can be performed for periodic devices with rather simple modifications of the basic algebraic formula associating the displacement and electrical fields to the boundary solicitations. Considering the harmonic excitation illustrated by Eq. (1), we relate all the degrees of freedom (DOFs) on boundary Γ_A to those on boundary Γ_B, yielding the following expression:

$$\begin{Bmatrix} u_{\Gamma_B} \\ \phi_{\Gamma_B} \end{Bmatrix} = \begin{Bmatrix} u_{\Gamma_A} \\ \phi_{\Gamma_A} \end{Bmatrix} e^{-j2\pi\gamma}, \tag{2}$$

in which u represents the mechanical displacements. This relation then is used to reduce the number of independent DOF of the FEA model. This is performed without changing the total number of DOF of the problem and simply by using a variable change operator C depending on the excitation parameter γ.[22] This provides the following form of the FEA algebraic system to be solved:

$$\begin{aligned} {}^t\begin{bmatrix} C_u^*(\gamma) & 0 \\ 0 & C_\phi^*(\gamma) \end{bmatrix} & \begin{bmatrix} K_{uu}-\omega^2 M_{uu} & K_{u\phi} \\ K_{\phi u} & K_{\phi\phi} \end{bmatrix} \\ & \times \begin{bmatrix} C_u(\gamma) & 0 \\ 0 & C_\phi(\gamma) \end{bmatrix} \begin{Bmatrix} v \\ \varphi \end{Bmatrix} = {}^t\begin{bmatrix} C_u^*(\gamma) & 0 \\ 0 & C_\phi^*(\gamma) \end{bmatrix} \begin{Bmatrix} F \\ Q \end{Bmatrix}, \end{aligned} \tag{3}$$

where K and M are the FEA stiffness and mass matrices, respectively,[22] ν and φ the independent DOFs of the problem, and F and Q the right hand side boundary forces and electrical charges. The superscript $*$ denotes a complex conjugation. Since K can be complex, the left hand side matrix in Eq. (3) is complex general (hermitic if $K \in \Re$) but sparse. These properties are considered when solving the problem. As explained in Ref. 22, algebraic system (3) is solved, allowing for the computation of the total electrical charge under active electrodes simply by nodal value summation. The harmonic (frequency and γ dependent) admittance then is equal to the electrode current for a unit voltage excitation ($\phi_0 = 1\ \text{V}$).

Let us now consider the case of acoustic radiation on one border of the meshed domain. In that purpose, the general variational equation is considered, limited to the purely elastic problem without any loss of generality,

$$\int_\Omega\int\int\left(\rho\omega^2 u_i \delta u_i^* - \frac{\partial \delta u_i^*}{\partial x_j} C_{ijkl} \frac{\partial u_l}{\partial x_k}\right) dV = \int_\Gamma\int \delta u_i^* T_{ij} n_j dS, \tag{4}$$

in which δu_i is the variational unknown and n_j the normal to the boundary Γ (bordering the domain Ω) on which the radiation boundary condition may partially occur. The mass density is represented by ρ and C_{ijkl} holds for the elastic constants. Equation (4) is written in three dimensions but of course its restriction to 2D problems does not induce any fundamental difficulty. The right hand side of Eq. (3) then is considered separately. In this matter, one can relate the dynamic stress T_{ij} to the displacement u_k in the spectral domain (denoted by $\sim$) by using Green's-function-based relation which generalizes the usual surface stress relation widely used in SAW modeling[2,8–11] as follows:

$$\tilde{T}_{ij} = \tilde{G}_{ijk}(s_1, \omega)\tilde{u}_k. \tag{5}$$

Note that in this equation, Green's function is the inverse of the one used by Ventura *et al.*,[2,12] and it asymptotically behaves like s_1 when s_1 tends to infinity. As demonstrated further, this does not generate numerical troubles. Equation (5) allows one for considering any flat boundary for the application of the radiation conditions, even if tilted in the plane (x_1, x_2). Using the now well-established periodic Green's-function formalism,[7] the right hand side of Eq. (4) is expressed as

$$\int_\Gamma\int \delta u_i^* T_{ij} n_j dS = \int_\Gamma\int \delta u_i^*(x) \sum_{l=-\infty}^{+\infty} G_{ijk}(\gamma + l, \omega)\frac{n_j}{p} e^{-j(2\pi/p)(\gamma+l)(x-x')} u_k(x') dx' dx \tag{6}$$

with p as the period of the problem and l as the number of the current space harmonic. The actual slowness s_1 is defined as $2\pi(\gamma+l)/p\omega$. The classical FEA interpolation procedure then is applied to Eq. (6), yielding the following expression of the boundary radiation operator:

$$\int_\Gamma\int \delta u_i^* T_{ij} n_j dS = \sum_{e,\varepsilon=1}^{E} \sum_{l=-\infty}^{+\infty} \frac{n_j}{p} G_{ijk}(\gamma + l, \omega) \times \int_{\Gamma e} \sum_{n=1}^{Nd(e)} P_n(x) e^{-j(2\pi/p)(\gamma+l)x} dx\, \delta u_i^{*(n,e)} \int_{\Gamma\varepsilon} \sum_{m=1}^{Nd(\varepsilon)} P_m(x') e^{j(2\pi/p)(\gamma+l)x'} dx'\, u_k^{(m,\varepsilon)}, \tag{7}$$

where E is the total number of "radiating" elements, $P_n(x)$ are the FEA interpolation polynomials (first or second degree), and $u_i^{(n,e)}$ is the discrete value of the displacement associated to the nth polynomial and nth DOF of the element e. Equation (7) can be finally written as

$$\int_\Gamma\int \delta u_i T_{ij} n_j dS = \sum_{e,\varepsilon=1}^{E} \sum_{n=1}^{Nd(e)} \sum_{m=1}^{Nd(\varepsilon)} \sum_{l=-\infty}^{+\infty} \frac{n_j}{p} G_{ijk}(\gamma + l, \omega) u_k^{(m,\varepsilon)} \delta u_i^{*(n,e)} I_{\gamma+l}^{*(n,e)} I_{\gamma+l}^{(m,\varepsilon)} \tag{8}$$

with $I_{\gamma+l}^{(m,\varepsilon)} = \int_{\Gamma\varepsilon} P_m(x) e^{j(2\pi/p)(\gamma+l)x} dx$ and with Γ_e as the actual radiation area of the element e. The integration of the interpolation polynomials times the exponential term $I_{\gamma+1}^{(m,\varepsilon)}$ generates terms in $p/2\pi(\gamma+l)$, which are homogeneous to $1/\omega s_1$ (i.e., to the actual wavelength). As a consequence, the expression of Eq. (8) behaves like $1/s_1$ when s_1 tends to infinity in the worst cases (i.e., the most important terms would be given by the integration of the constants of the interpolation polynomials). Hence, the computation of the radiation contribution via the development of Eq. (8) converges even for large number of space harmonics. Practically, we have pointed out an optimum between the number of radiating elements and the space harmonics allowing for a systematic convergence, which is discussed further.

The contribution of the total radiating boundary to the global algebraic system to be solved then consists in a frequency and excitation parameter dependent matrix $X(\omega, \gamma)$ related to both DOF and variational unknowns and consequently computed in the left hand side of Eq. (3) as reported in the following equation describing a general piezoelectric problem:[22]

$$
{}^{t}\begin{bmatrix} C_u^*(\gamma) & 0 \\ 0 & C_\phi^*(\gamma) \end{bmatrix}\left(\begin{bmatrix} K_{uu}-\omega^2 M_{uu} & K_{u\phi} \\ K_{\phi u} & K_{\phi\phi} \end{bmatrix} - \begin{bmatrix} X_{uu}(\omega,\gamma) & X_{u\phi}(\omega,\gamma) \\ X_{\phi u}(\omega,\gamma) & X_{\phi\phi}(\omega,\gamma) \end{bmatrix}\right)\begin{bmatrix} C_u(\gamma) & 0 \\ 0 & C_\phi(\gamma) \end{bmatrix}\begin{Bmatrix} v \\ \varphi \end{Bmatrix} = {}^{t}\begin{bmatrix} C_u^*(\gamma) & 0 \\ 0 & C_\phi^*(\gamma) \end{bmatrix}\begin{Bmatrix} F \\ Q \end{Bmatrix}. \tag{9}
$$

Even for materials without any losses, this algebraic system is general complex without any specific mathematical characteristics. Also the sparse nature of the algebraic system is degraded due to the connection of all the DOF one to the other via the radiation coupling.

III. NUMERICAL IMPLEMENTATION

A. General discussion

In this section, a particular interest is dedicated to the properties of the different terms involved in the computation of Eq. (9) and a strategy is proposed to reduce computation duration. In Eq. (8), it appears that the two boundary integrals are complex conjugated, potentially yielding hermitic properties of the matrix. However, the parity properties of Green's function[23] prevent any simplification of the calculation. It is then necessary to compute all the terms of Eq. (8). However, it is relevant to compute the integral $I_{\gamma+l}^{(m,\varepsilon)}$ for all the possible values of $\gamma+l$ and for all the radiating elements and also to compute Green's tensor for all $\gamma+l$ and ω before assembling the radiation matrix $X(\omega,\gamma)$ which can be performed just before solving the system. Note that this assembly cannot be performed in the usual FEA approach in which elementary matrices are summed to build K and M. In the present case, the nonsymmetric sparse matrix is directly built computing all the cross-coupled terms induced by the convolution between the unknown fields and Green's function for each frequency.

In Eqs. (6)–(8), an infinite sum over the space harmonics is performed to compute Green's function. Practically, the sum is reduced to a finite number of terms (from a few tenths to 100 typically) to ensure the convergence of the calculation. Empirically, we found out that the number of harmonics should be at least equal to half the number of elements of the radiation boundary. A specific treatment of the asymptotic behavior of Green's function is currently investigated, which should allow us to reduce this number. On the other hand, it is not obvious to establish whether the computation duration gain offered by such a treatment will be as high as in the case of the mixed FEA-BIM approach[2] for which the specific treatment of Green's-function asymptotic behavior reduces the computation duration by more than a scale order (typically ten space harmonics[2] instead of more than 100 without asymptotic treatment[9]). Finally, the radiation medium can be composed of any combination of dielectrics, fluids, and even metallic domains (assuming flat interfaces),[17] taking advantage of the stabilization of Green's function described in Ref. 24.

The last aspect of the model discussed here concerns the number of DOF in the FEA development. Generally, purely elastic 2D-FEA simulations are performed using finite element exhibiting two DOFs, as it sounds natural to consider displacements along the leading axes of the considered plane. In our case, we assume that the metal strips are infinite along the normal to the saggital plane, then corresponding to the so-called plane-deformation configuration. We also assume the possible existence of shear displacements along the normal to that plane (but described in the saggital plane) and the associated electric potential. We then have developed different finite elements allowing for considering any particular situation, allowing for optimized matrix size of Eq. (9) and hence reduced computation delays. In the case of generally polarized waves, the whole displacement field and its associated electrical potential then can be considered on the FEA part and the BEM as well, yielding high accuracy prediction and large computation delays. For quasisaggital waves such as Rayleigh waves on singly rotated quartz cuts (propagation along X axis), we may consider a displacement field reduced to saggital terms $\tilde{u}_1$ and $\tilde{u}_2$ in the FEA (plus of course the dynamical potential $\tilde{\phi}$). However, a weak but existing coupling arises along the normal to the saggital plane, which must be accounted for to reach the standard Rayleigh wave prediction accuracy.[2] If we assume that only the saggital terms play a role at the electrode/crystal interface (the shear displacement of the wave $\tilde{u}_3$ is more than ten times smaller than its elliptic components), we then consider the continuity of the surface stress and displacements at this interface, yielding the following boundary conditions considering the saggital plane (x_1,x_2) and the propagation direction along x_1:

$$
\tilde{T}_{12}^{\text{elec}} = \tilde{T}_{12}^{\text{cryst}}, \quad \tilde{T}_{22}^{\text{elec}} = \tilde{T}_{22}^{\text{cryst}}, \quad \tilde{T}_{32}^{\text{cryst}} = 0, \quad D_2^{\text{cryst}} = Q,
$$

$$
\tilde{u}_1^{\text{elec}} = \tilde{u}_1^{\text{cryst}}, \quad \tilde{u}_2^{\text{elec}} = \tilde{u}_2^{\text{cryst}}, \quad \phi^{\text{cryst}} = \phi^0 \tag{10}
$$

and no condition is applied on $\tilde{u}_3$. Using Eq. (5), it is possible to express $\tilde{u}_3$ as a combination of Green's matrix elements and displacements u_1 and u_2 using the condition $\tilde{T}_{32}^{\text{cryst}}=0$. This reads

$$
\tilde{u}_3 = -\frac{\tilde{G}_{321}}{\tilde{G}_{323}}\tilde{u}_1 - \frac{\tilde{G}_{322}}{\tilde{G}_{323}}\tilde{u}_2 - \frac{\tilde{G}_{324}}{\tilde{G}_{323}}\tilde{\phi}. \tag{11}
$$

Considering now Eq. (11), we can write Green's function to insert in the BEM as follows:

$$
\tilde{T}_{12} = \frac{\tilde{G}_{121}\tilde{G}_{323} - \tilde{G}_{123}\tilde{G}_{321}}{\tilde{G}_{323}}\tilde{u}_1 + \frac{\tilde{G}_{122}\tilde{G}_{323} - \tilde{G}_{123}\tilde{G}_{322}}{\tilde{G}_{323}}\tilde{u}_2 + \frac{\tilde{G}_{124}\tilde{G}_{323} - \tilde{G}_{123}\tilde{G}_{324}}{\tilde{G}_{323}}\tilde{\phi},
$$

$$
\tilde{T}_{22} = \frac{\tilde{G}_{221}\tilde{G}_{323} - \tilde{G}_{223}\tilde{G}_{321}}{\tilde{G}_{323}}\tilde{u}_1 + \frac{\tilde{G}_{222}\tilde{G}_{323} - \tilde{G}_{223}\tilde{G}_{322}}{\tilde{G}_{323}}\tilde{u}_2 + \frac{\tilde{G}_{224}\tilde{G}_{323} - \tilde{G}_{223}\tilde{G}_{324}}{\tilde{G}_{323}}\tilde{\phi},
$$

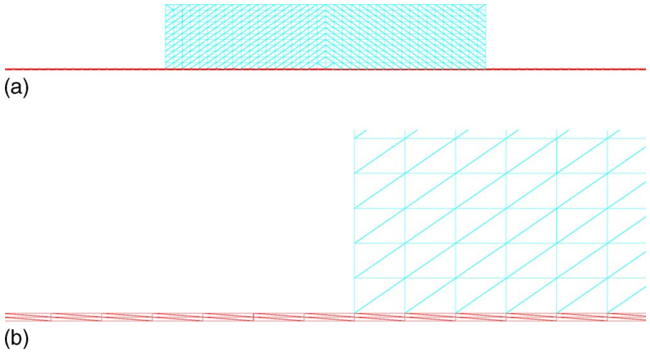

FIG. 2. (Color online) Meshes used for the validation computations. The period p is fixed to 5 μm, the metallization ratio $a/p=0.5$, and relative electrode height $0<h<5\%$ (here $h=500$ nm). (a) Global view of the mesh; (b) close view of the strip edge.

$$\tilde{T}_{24}=\tilde{D}_2=\frac{\tilde{G}_{421}\tilde{G}_{323}-\tilde{G}_{423}\tilde{G}_{321}}{\tilde{G}_{323}}\tilde{u}_1+\frac{\tilde{G}_{422}\tilde{G}_{323}-\tilde{G}_{423}\tilde{G}_{322}}{\tilde{G}_{323}}\tilde{u}_2+\frac{\tilde{G}_{424}\tilde{G}_{323}-\tilde{G}_{423}\tilde{G}_{324}}{\tilde{G}_{323}}\tilde{\phi}. \tag{12}$$

We show further the efficiency of this correction. If we now consider the case of quasi-shear-surface wave as propagating atop lithium tantalate $(YXl)/42°$, the same kind of correction must be applied to only consider $\tilde{u}_3$ and $\tilde{\phi}$ as the only DOFs of the FEA part of the problem. In that case, $\tilde{T}_{12}^{\text{cryst}}=\tilde{T}_{22}^{\text{cryst}}=0$, yielding a system of equation allowing to write $\tilde{u}_1$ and $\tilde{u}_2$ as a function of $\tilde{u}_3$ and $\tilde{\phi}$ (see Appendix). We then obtain Green's matrix of rank 2 with corrected parameters in a similar way to the one presented above for Rayleigh waves.

B. Numerical tests

The proposed theoretical development has been implemented and a first set of computation tests has been performed considering the excitation of Rayleigh and STWs on AT quartz cut and leaky surface waves on $(YXl)/42°$ LiTaO$_3$ cut. The polarization of the waves propagating atop these substrates is either mainly elliptical or mainly transverse, but an accurate description of their properties may impose to account for a comprehensive displacement field (and its associated potential of course). The computation results are compared to those provided by the well-known mixed finite element/boundary integral approach proposed by Ventura *et al.*[2] Different electrode configurations have been considered as shown further. The simplest mesh used to compute the standard single electrode problem is plotted in Fig. 2. The period p of the grating was arbitrarily fixed to 5 μm, the metal ratio $a/p=0.5$, and the relative aluminum thickness was varied from 0 to 5% for quartz (electrode height h ranging from 0 to 500 nm). The number of elements has been adapted depending on the electrode height (about two layers of elements for each 50 nm height), but the number of radiating element along the period was kept identical for all computations. As shown in Fig. 2, only a small part of the semi-infinite medium has to be meshed, yielding rather short computation delays (but longer than those of FEA-BIM approaches[2]). Note that the position of the electrode center has no influence on the computation results. Material constants used for the computations are these of Slobodnik *et al.*[25] for quartz and these of Kovacs *et al.*[26] for lithium tantalate, respectively. Data for aluminum electrodes can be found, for instance, in Ref. 27. In the case of quartz, we account for the dielectric contribution of vacuum directly in Green's function (as in Refs. 2, 4, 11, and 12), whereas this contribution is negligible for materials with larger dielectric properties such as LiTaO$_3$.

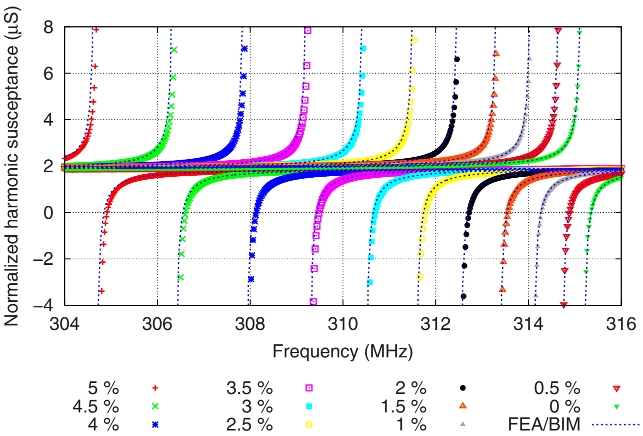

FIG. 3. (Color online) Comparison between the harmonic admittance computed with the FEA-BIM approach by Ventura *et al.* (Ref. 2) and the proposed method at $\gamma=0.5$, $a/p=0.5$, h/λ varying from 0 to 5% by step of 0.5% ($p=5$ μm), dependence vs ω, and imaginary part of the harmonic admittance of a Rayleigh wave on $(YXl)/36°$ quartz (dashed blue: FEA-BIM; points: this work).

Figure 3 shows a comparison between the well-established FEA-BIM model[2] and the present work's results for a Rayleigh wave propagating atop AT cut quartz (propagation along X axis) and an excitation condition γ equal to 1/2. In that case, the convergence was found using 40 nodes at the interface electrode/substrate together with 80 spatial harmonics (76 elements along the period). It occurs as soon as the number of spatial harmonics overcomes the number of boundary elements (empirically). Elements with four DOFs (u_1, u_2, u_3, and ϕ) have been used for these computations,

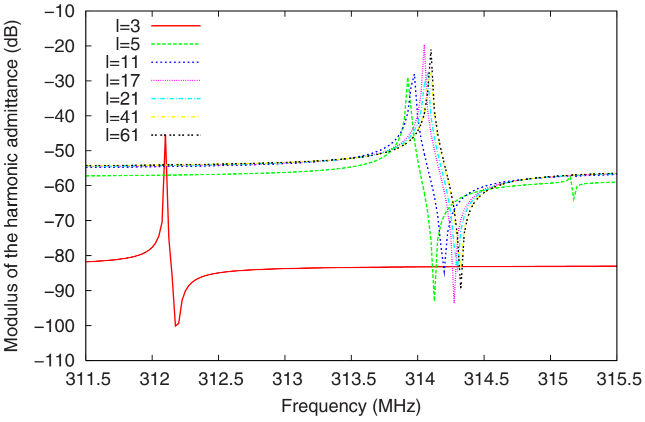

FIG. 4. (Color online) Influence of the space harmonic number on the accuracy of the harmonic admittance computation, $\gamma=0.5$, $a/p=0.5$, and $h/\lambda=1\%$. Convergence is reached for 41 harmonics ($l=-20-+20$).

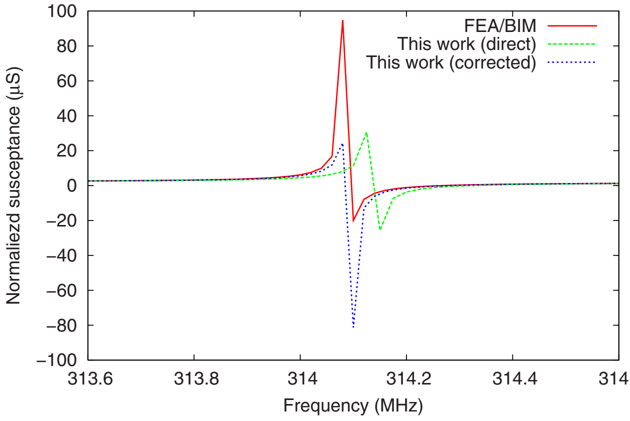

FIG. 5. (Color online) Superposition of harmonic admittance computed using our FEA-BEM formulation with noncorrected and corrected Green's functions, Rayleigh wave on $(YXl)/36°$ quartz, $\gamma=0.5$, $a/p=0.5$, and $h/\lambda=1\%$ ($p=5$ μm). Comparison with FEA-BIM results, emphasizing the efficiency of the correction.

the potential being forced to 1 V at the electrode boundaries. The stability of the computation also has been tested: the number of harmonics does not affect the result once the convergence is met (as shown in Fig. 4). Also note that only two element layers (total thickness of 10 nm) were required to operate the matching between FEA and BEM formulations. This suggests that the influence of this matching mesh is quite weak on the computation results and that it eventually could be suppressed in further developments. We also have tested the efficiency of Green's-function correction for the use of three DOF piezoelectric elements instead of the previously used four DOF ones. Figure 5 shows the superposition of the FEA-BIM results with those obtained using our FEA-BEM formulation with noncorrected (i.e., simply suppressing the radiation terms corresponding to $\tilde{u}_3$) and corrected Green's functions in the case of Rayleigh waves on (AT,*X*) quartz. The efficiency of the correction here is clearly emphasized.

The sensitivity of the STW resonance to mass loading also was checked (propagation along rotated *Z* axis on AT cut quartz) and compared to FEA-BIM computation results, as reported in Fig. 6. Note that in this case too, we achieve a good agreement between our results and those provided by the FEA-BIM approach using first order interpolation polynomials and two DOF finite elements (u_3 and ϕ), which are both favorable for fast computations. Contrarily to what expected, the use of second order interpolation polynomials did not provide any substantial reduction in the computation delay. This problem needs further inspection which overcomes the scope of this paper.

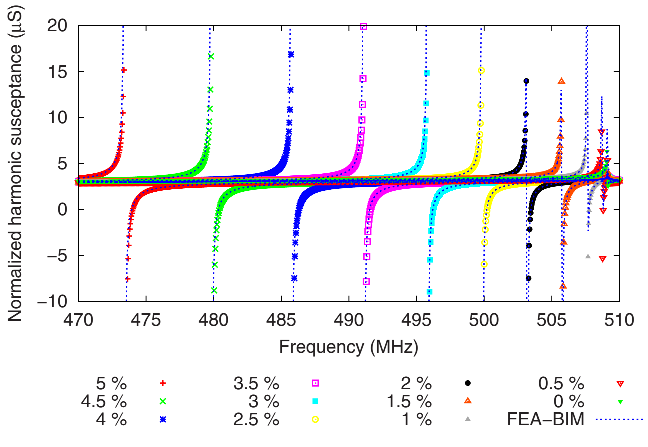

FIG. 6. (Color online) Comparison between the harmonic admittance computed with the FEA-BIM approach by Ventura *et al.* (Ref. 2) and the proposed method at $\gamma=0.5$, $a/p=0.5$, h/λ varying from 0 to 5% by step of 0.5% ($p=5$ μm), dependence vs ω, and imaginary part of the harmonic admittance of a STW on $(YXlt)/36°/90°$ quartz (dashed blue: FEA-BIM; points: this work).

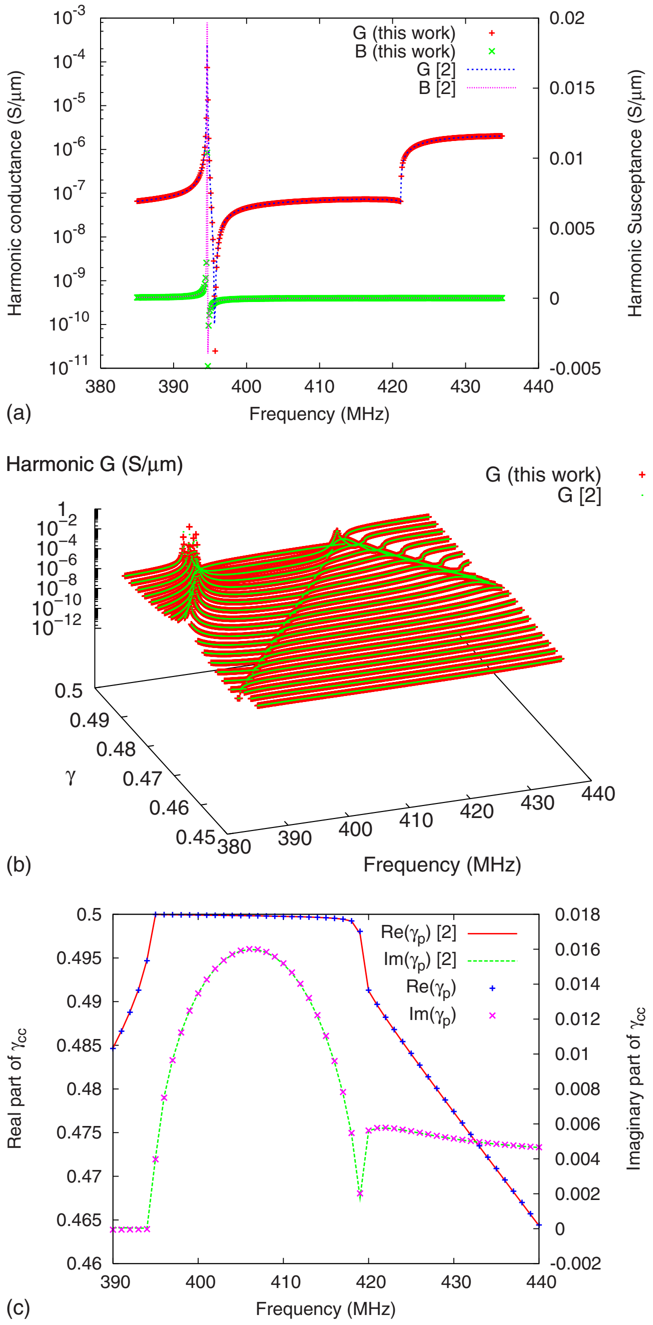

FIG. 7. (Color online) Validation of the accuracy of the proposed approach for a PSAW on $(YXl)/42°$ LiTaO$_3$ (a) dependence vs ω, $\gamma=0.5$, imaginary part of the harmonic admittance (solid green: FEA-BIM dots; blue: this work). (b) Comparison between dispersion curves provided by the two considered models (solid green: FEA-BIM dots; blue: this work). (c) Fit of the propagation parameters of the wave in the frequency stop-band region for a thick electrode array ($h/\lambda=8\%, a/p=0.5$) (lines: FEA-BIM; crosses: this work).

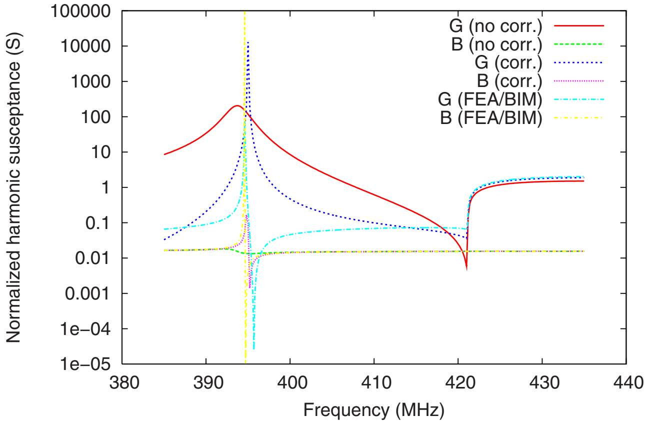

FIG. 8. (Color online) Superposition of harmonic admittance computed using our FEA-BEM formulation with noncorrected and corrected Green's functions, PSAW on $(YXl)/42°$ LiTaO$_3$, $\gamma=0.5$, $a/p=0.5$, and $h/\lambda=8\%$ ($p=5$ μm). Comparison with FEA-BIM results, emphasizing the effect of the correction.

Figure 7 shows the comparison between harmonic admittances computed in the vicinity of the frequency stop band for the leaky shear wave on $(YXl)/42°$ LiTa0$_3$ with a metal thickness close to the one allowing for leakage suppression,[9] i.e., $h/\lambda=8\%$. Once again, the agreement between the proposed model results and those provided by the FEA-BIM approach is almost perfect, whatever the value of the excitation parameter γ [Fig. 7(b)]. A two point fit conform to the one implemented in Ref. 28 has been implemented to accurately characterize the frequency stop band of the mode. Once again, the results obtained using the present development nicely fit those provided by the method of Ventura *et al.*,[2] as shown in Fig. 7(c), showing that the characterization of the frequency stop band enabling the wave parameter extraction can be achieved in a very comparable way for both approaches. We also have checked the possibility to reduce the number of DOF in the FEA part of the problem using corrected Green's-function-based BEM. As shown in Fig. 8, this approach was found efficient but not as much as for Rayleigh waves on singly rotated quartz cuts. There is clearly an improvement in the admittance prediction when using the corrected form of Green's function (see Appendix), particularly concerning the propagation losses but the position of the pseudopole is not absolutely coincident with the one predicted using the complete acoustic field (FEA/BIM approaches or this work, as shown in Fig. 7). This means that in this particular case, one cannot neglect the contribution of the saggital acoustic field in the electrode to the wave guidance.

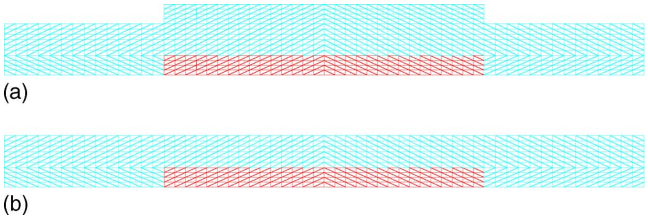

FIG. 10. (Color online) Meshes of a passivated electrode grating device with (a) conformal and (b) nonconformal depositions, $p=5$ μm, $a/p=0.5$, and $h/\lambda=1,5\%$ (STW synchronous transducer covered by a 400 nm amorphous silica—blue part of the mesh: SiO$_2$; orange part: Al).

The possibility to reduce the number of DOF for pure shear waves however was checked for pure transverse wave on quartz (Fig. 6). We found out however that in that case, the correction of Green's function is not needed as there is absolutely no coupling between saggital displacement components (u_1,u_2) and the shear displacement component u_3 and its associated potential ϕ.

IV. APPLICATION TO MORE COMPLEX ELECTRODE GEOMETRIES

A. Passivated structures

Passivation layers are used to protect the surface of SAW devices from any dusts or surface pollution that could counteract the IDT operation. Generally, very thin dielectric films are deposited atop the device to be passivated but even such a very thin overlay may significantly modify the SAW properties. To illustrate the capability of our model to correctly predict the response of complex surface structures, we have theoretically and experimentally check the influence of an amorphous silica (SiO$_2$) coating on a two port STW resona-

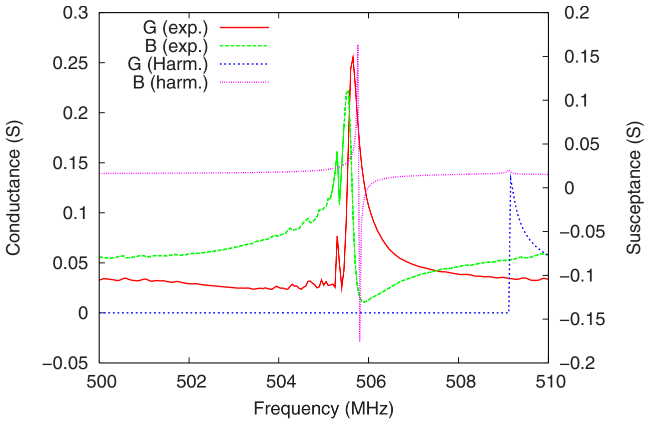

FIG. 9. (Color online) Superposition of harmonic admittances computed using the present approach with the experimentally measured admittance of one of four-port STW resonator IDTs (grating period $p=5$ μm, relative electrode height $h/\lambda=1.5\%$, and metallization ratio $a/p=0.5$).

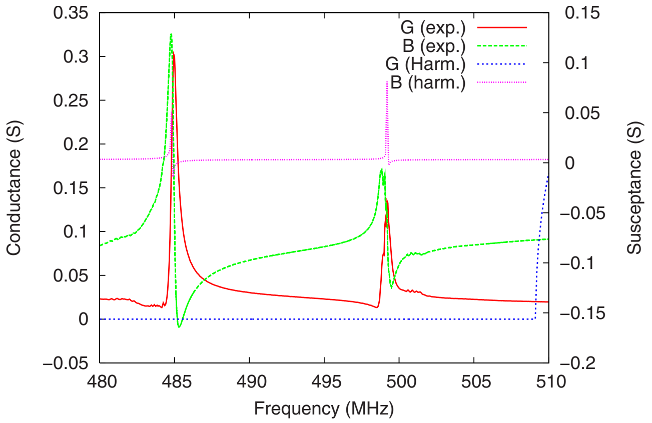

FIG. 11. (Color online) Superposition of harmonic admittances computed using the present approach and meshes of Fig. 10 with the experimentally measured admittance of a passivated four-port STW resonator IDT built using parameters reported in caption of Fig. 10 (Ref. 29).

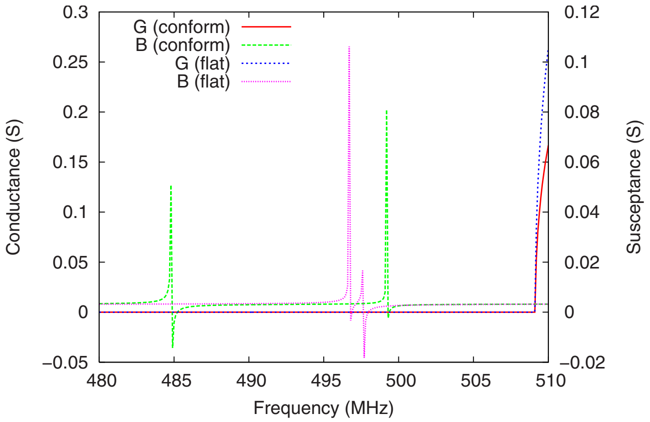

FIG. 12. (Color online) Comparison between harmonic admittances of conformal and nonconformal SiO_2 passivated STW gratings.

tor. These devices developed for sensor applications[29] consist in a four-port STW synchronous resonator operating close to 500 MHz (grating period $p=5$ μm, relative electrode height $h/\lambda=1.5\%$, metallization ratio $a/p=0.5$) built on AT cut of quartz (propagation along Z′) covered by a 0.4 μm thick amorphous silica layer. The initial resonator exhibits a single contribution near 506 MHz, as attested by the experimental admittance of one of the device transducers (see Fig. 9). This contribution is correctly predicted by our model, as proven by the superposition of the experimental and harmonic admittances. The final resonator presents two resonances corresponding, respectively, to the beginning and the end of the frequency stop band. The stop-band width only can be accurately predict if considering a conformal deposition, i.e., the corrugation due to the metal strip is reproduced at the silica surface. This is illustrated by Fig. 10(a) showing the mesh used to perform these computations. A comparison between the harmonic admittance and the transfer function of the abovementioned resonator is reported in Fig. 11, showing a good agreement between theory and experiment. The harmonic admittance of a flat surface passivated device is also reported in Fig. 12 [using the mesh of Fig. 10(b)], emphasizing a stop band much smaller than the one actually measured. This shows the need to accurately take into account the actual form of the grating to correctly predict the characteristics of the device and hence the interest of the proposed model.

B. Prominent electrode structures

We also have chosen to address the problem of STWs under prominent electrode gratings for which experimental data were available.[20] This structure was built by etching the quartz in between the electrodes of a four-port synchronous STW resonator, yielding mixed strip-and-groove gratings and IDTs. We compare the experimental resonance frequencies f_r and stop bandwidth Δf measured on synchronous resonators with harmonic admittances obtained using our FEA/BEM approach. The typical mesh for prominent electrode gratings is plotted in Fig. 13.

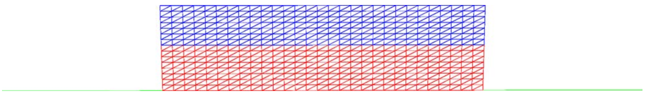

FIG. 13. (Color online) Mesh of the considered prominent electrode grating device (Ref. 20) (red part of the mesh: quartz; blue part: Al; and green section: interface between FEA and BEM).

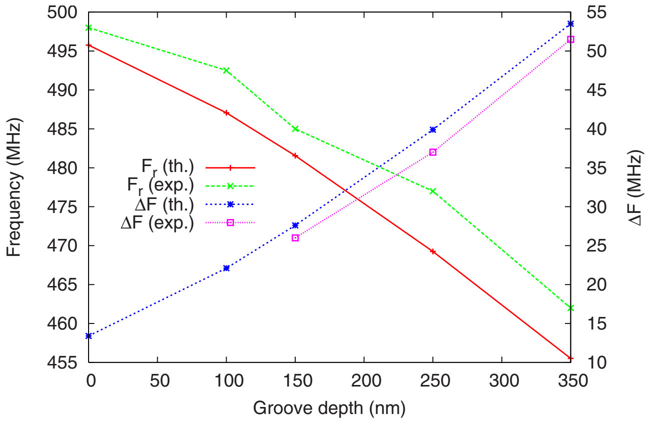

FIG. 14. (Color online) Comparison between theoretical and experimental resonance frequency and stop bandwidth for prominent electrode grating based resonators (Ref. 20).

Again in that case, the grating's period was 5 μm with a metallization ratio of 0.5. The strip height atop the resulting prominent quartz ridge was 300 nm with a groove depth ranging from 0 to 350 nm. We measured both resonance frequency and frequency stop-band width in that case, and a comparison with theoretical results is reported in Fig. 14, emphasizing a good prediction of the behavior of the device (good accordance between the predicted and measured shapes of the curves).

V. CONCLUSION

A model combining periodic FEA and a BEM has been developed and implemented to address the problem of elastic wave guides exhibiting complicated forms and material combinations. The convergence conditions have been identified and reported considering the numerous parameters of the approach (elements, interpolation, space harmonics, wave polarization, etc.). The results provided by the proposed approach have been compared to well-established models and were found to provide accurate predictions whatever the nature of the wave (Rayleigh SAW, leaky SAW, and pure transverse wave). It was applied to analyze passivated and recessed electrode grating based devices, showing the interest of the approach. Many developments now can be investigated, starting from this basis. Applications to interface waves, immersed sensors, as well as three-dimensional (3D) transducers are on the way. Multiple electrode gratings (for instance, distributed acoustic resonant transducers) can be addressed as well. Also it will be very interesting to try and investigate the possibility to mix finite structure boundary conditions with periodic ones to address the problem of 3D IDT modeling.

ACKNOWLEDGMENTS

This paper is dedicated to all the people who have contributed to settle the close collaboration between the LPMO

Laboratory and TMX-TEMEX for about 12 years, D. Hauden and J.-J. Gagnepain on the CNRS side and Ch. Maerfeld and P. Tournois on the TMX side. Many thanks to J.-M. Hodé, J. Desbois, P. Ventura, M. Solal, M. Doisy, J. F. Gelly, and G. Vanderborck for so many fruitful discussions on the subject.

APPENDIX: CORRECTION OF GREEN'S MATRIX FOR A TWO DOF FEA FORMULATION OF QUASI-SHEAR-WAVE PROPAGATION

We consider here that only the shear terms play a role at the electrode/crystal interface, but a weak coupling of $\tilde{u}_1$ and $\tilde{u}_2$ exists that must be consider for an accurate estimation of the wave velocity under the grating. This is the case of quasi-shear-surface wave as propagating atop lithium tantalate $(YXl)/42°$. The following correction must be applied to only consider $\tilde{u}_3$ and $\tilde{\phi}$ as the only DOF of the FEA part of the problem. In that case, the following boundary conditions must be considered:

$$\tilde{T}_{12}^{\text{elec}} = 0, \quad \tilde{T}_{22}^{\text{elec}} = 0, \quad \tilde{T}_{32}^{\text{elec}} = \tilde{T}_{32}^{\text{cryst}}, \quad D_2^{\text{cryst}} = Q,$$

$$\tilde{u}_3^{\text{elec}} = \tilde{u}_3^{\text{cryst}}, \quad \phi^{\text{cryst}} = \phi^0 \tag{A1}$$

and no condition is applied on $\tilde{u}_1$ and $\tilde{u}_2$. Using Eq. (A1), we express them as a combination of Green's matrix elements and $\tilde{u}_3$ and $\tilde{\phi}$ as shown in Sec. III A for elliptical polarization. Developing $\tilde{T}_{12}^{\text{cryst}}=\tilde{T}_{22}^{\text{cryst}}=0$ yields the following system:

$$\begin{aligned} \tilde{G}_{121}\tilde{u}_1 + \tilde{G}_{122}\tilde{u}_2 &= -\tilde{G}_{123}\tilde{u}_3 - \tilde{G}_{124}\tilde{\phi}, \\ \tilde{G}_{221}\tilde{u}_1 + \tilde{G}_{222}\tilde{u}_2 &= -\tilde{G}_{223}\tilde{u}_3 - \tilde{G}_{224}\tilde{\phi}. \end{aligned} \tag{A2}$$

Solving this system provides the relation we are looking for,

$$\begin{aligned} \tilde{u}_1 &= \frac{(\tilde{G}_{122}\tilde{G}_{223} - \tilde{G}_{123}\tilde{G}_{222})\tilde{u}_3 + (\tilde{G}_{122}\tilde{G}_{224} - \tilde{G}_{124}\tilde{G}_{222})\tilde{\phi}}{\det}, \\ \tilde{u}_2 &= \frac{(\tilde{G}_{221}\tilde{G}_{123} - \tilde{G}_{223}\tilde{G}_{121})\tilde{u}_3 + (\tilde{G}_{221}\tilde{G}_{124} - \tilde{G}_{121}\tilde{G}_{224})\tilde{\phi}}{\det}, \\ \det &= \tilde{G}_{121}\tilde{G}_{222} - \tilde{G}_{221}\tilde{G}_{122}. \end{aligned} \tag{A3}$$

Considering now Eq. (A3), we can write Green's function to insert in the BEM as follows:

$$\begin{aligned} \tilde{T}_{32} &= \frac{\tilde{G}_{321}(\tilde{G}_{122}\tilde{G}_{223} - \tilde{G}_{123}\tilde{G}_{222}) + \tilde{G}_{322}(\tilde{G}_{221}\tilde{G}_{123} - \tilde{G}_{223}\tilde{G}_{121}) + \tilde{G}_{323}\det}{\det}\tilde{u}_3 \\ &\quad + \frac{\tilde{G}_{321}(\tilde{G}_{122}\tilde{G}_{224} - \tilde{G}_{124}\tilde{G}_{222}) + \tilde{G}_{322}(\tilde{G}_{221}\tilde{G}_{124} - \tilde{G}_{121}\tilde{G}_{224}) + \tilde{G}_{324}\det}{\det}\tilde{\phi}, \\ \tilde{T}_{24} = \tilde{D}_2 &= \frac{\tilde{G}_{421}(\tilde{G}_{122}\tilde{G}_{223} - \tilde{G}_{123}\tilde{G}_{222}) + \tilde{G}_{422}(\tilde{G}_{221}\tilde{G}_{123} - \tilde{G}_{223}\tilde{G}_{121}) + \tilde{G}_{423}\det}{\det}\tilde{u}_3 \\ &\quad + \frac{\tilde{G}_{421}(\tilde{G}_{122}\tilde{G}_{224} - \tilde{G}_{124}\tilde{G}_{222}) + \tilde{G}_{422}(\tilde{G}_{221}\tilde{G}_{124} - \tilde{G}_{121}\tilde{G}_{224}) + \tilde{G}_{424}\det}{\det}\tilde{\phi}. \end{aligned} \tag{A4}$$

[1] H. Engan, IEEE Trans. Electron Devices **16**, 1014 (1969).

[2] P. Ventura, J. M. Hode, and M. Solal, Proc.-IEEE Ultrason. Symp. **1**, 263 (1995).

[3] K. Blötekjaer, K. A. Ingebrigsten, and H. Skeie, IEEE Trans. Electron Devices **20**, 1133 (1973).

[4] Y. Zhang, J. Desbois, and L. Boyer, IEEE Trans. Ultrason. Ferroelectr. Freq. Control **40**, 183 (1993).

[5] H. Reichinger and A. R. Baghai-Wadji, Proc.-IEEE Ultrason. Symp. **1**, 7 (1992).

[6] H. P. Zideck, A. R. Baghaï-Wadji, and O. Manner, Proc.-IEEE Ultrason. Symp. **1**, 149 (1993).

[7] V. P. Plessky and T. Thorvaldsson, Electron. Lett. **28**, 1317 (1992).

[8] G. Endoh, K. Hashimoto, and M. Yamagushi, Jpn. J. Appl. Phys., Part 1 **34**, 2632 (1995).

[9] J. Koskela, V. P. Plessky, and M. M. Salomaa, IEEE Trans. Ultrason. Ferroelectr. Freq. Control **45**, 439 (1998).

[10] S. V. Biryukov and M. Weinhardt, J. Appl. Phys. **96**, 3117 (2004).

[11] S. Ballandras, A. Reinhardt, V. Laude, A. Soufyane, S. Camou, W. Daniau, T. Pastureaud, W. Steichen, R. Lardat, M. Solal, and P. Ventura, J. Appl. Phys. **96**, 7731 (2004).

[12] P. Ventura, J. M. Hodé, J. Desbois, and M. Solal, IEEE Trans. Ultrason. Ferroelectr. Freq. Control **48**, 1259 (2001).

[13] S. Ballandras, G. Pierre, F. Blanc, P. F. Edoa, and W. Steichen, Proc.-IEEE Ultrason. Symp. **2**, 957 (1999).

[14] S. Ballandras, E. Bigler, W. Daniau, J. Py, A. Pakfar, G. Marianneau, and G. Martin, Proc.-IEEE Ultrason. Symp. **1**, 217 (1998).

[15] S. Kakio, K. Hishinuma, and Y. Nakagawa, J. Appl. Phys. **87**, 1440 (2000).

[16] T. Pastureaud, R. Lardat, W. Steichen, and P. Ventura, Proc.-IEEE Ultrason. Symp. **1**, 683 (2005).

[17] K. Shimoe and A. Hiraishi, Japanese Patent No. JP8265089 (A) (11 October 1996).

[18] A. Reinhardt and V. Th Pastureaud, J. Appl. Phys. **94**, 6923 (2003).

[19] S. Camou, V. Laude, Th. Pastureaud, and S. Ballandras, IEEE Trans. Ultrason. Ferroelectr. Freq. Control **50**, 1363 (2003).

[20] W. Daniau, S. Ballandras, and J. B. Briot, Proceedings of the IEEE IFCS, 1997 (unpublished), pp. 800–806.

[21] P. Langlet, A. C. Hladky-Henion, and J. N. Decarpigny, J. Acoust. Soc. Am. **98**, 2792 (1995).

[22] S. Ballandras, M. Wilm, P. F. Edoa, V. Laude, A. Soufyane, W. Steichen, and R. Lardat, J. Appl. Phys. **93**, 702 (2003).

[23] J.-M. Hodé and J. Desbois, Proc.-IEEE Ultrason. Symp. **1**, 131 (1999).

[24] Th. Pastureaud, V. Laude, and S. Ballandras, Appl. Phys. Lett. **80**, 2544 (2002).

[25] A. J. Slobodnik, E. D. Conway, R. T. Delmonico, and Air Force Cambridge Research Labs, *Microwave Acoustics Handbook*, Surface Wave Velocities Vol. 1A (Acoustical Society of America, New York, 1973).

[26] G. Kovacs, M. Anhorn, H. E. Engan, G. Visintini, and C. C. W. Ruppel, Proc.-IEEE Ultrason. Symp. **1**, 435 (1990).

[27] *Numerical Data and Functional Relationships in Science and Technology, Crystal and Solid State Physics*, Landolt-Börnstein, New Series, Group III, Vol. 11, edited by K. H. Hellwege and A. M. Hellwege (Springer-Verlag, Berlin, 1979).

[28] Y. Fusero, S. Ballandras, J. Desbois, J. M. Hodé, and P. Ventura, IEEE Trans. Ultrason. Ferroelectr. Freq. Control **49**, 805 (2002).

[29] S. Ballandras, M.H. Nadal, W. Daniau, V. Blondeau-Patissier, G. Martin, V. Eyraud, D.Hauden, B. Guichardaz, L. Hairault, B. Lebret, P. Blind, Proceedings of the Joint EFTF-IEEE IFCS, Tampa Bay, 2003 (unpublished), pp. 927–930.